Dual Delay-Compensation-Based Model Predictive Control for the Semi-Controlled Open-Winding PMSM System

XIAOGUANG ZHANG [1], **(Member, IEEE), KEQIN WANG[2], WENHAN ZHANG[1],**
YAOQIANG WANG [3]**, PENG WANG[1] AND DAWEI GAO** [4]**, (Member, IEEE)**

[1]College of Electrical and Control Engineering, North China University of Technology, Beijing 100144, China
[2]Jing-Jin Electric, Beijing 100144, China
[3]College of Electrical Engineering, Zhengzhou University, Zhengzhou 450001, China
[4]Department of Electrical Engineering, Tsinghua University, Beijing 100084, China

Corresponding author: Xiaoguang Zhang (zhangxg123456789@163.com)

ABSTRACT To improve the control performance of the semi-controlled open-end winding permanent magnetic synchronous motor (SOEW-PMSM) control system, a novel prediction control method is presented in this paper. First, the current–voltage dual delay-compensation algorithm is presented to overcome the negative influence on the steady-state performance of the whole control system. Then, in order to implement the simultaneous control of the d-axis current, the q-axis current, and the zero-sequence current, the current-error-based cost function is designed. Additionally, to further improve the control performance and decrease the calculation complexity of the prediction algorithm, controllable converter vector optimization-based prediction control method is presented. The effectiveness of the proposed prediction methods is tested by the simulation and experimental results.

INDEX TERMS Delay-compensation algorithm, model predictive control, computation burden reduction.

I. INTRODUCTION

Recently, since the advantages of multilevel output, excellent fault-tolerant ability and the current independent control, open-end winding permanent magnetic synchronous motor (OEW-PMSM) has obtained a wide range of concerns [1]–[3]. Usually, two converters are adopted to drive OEW-PMSM [4]–[7]. And many control methods and modulation strategies are proposed to optimize control characteristics, for example, dual-space vector control [8], optimal pulsewidth modulation method [9], torque/flux control and prediction control [10], [11].

It should be noted that recently some new developments for the control of OEW-PMSM system have been obtained. In [21], a q-axis current injection method based on angle-shift based voltage distribution is proposed for the OEW-PMSM drives with common dc bus, which can effectively reduce the

The associate editor coordinating the review of this manuscript and approving it for publication was Madhav Manjrekar.

torque ripple caused by zero-sequence current. In [22], an improvised SVPWM strategy for a four-level open-end winding induction motor drive is presented to enhance the system control performance. A different modulation strategy is presented in [24] to obtain lower switching frequency. In this method, one converter held clamped state and the other modulated based on the redistribution of the zero voltage vectors. In [23], a unified SVPWM strategy is presented for OEW-PMSM system with two isolated dc sources. This method can simplify the region identification in sectors and reduce total switching frequency of the dual inverter. In order to achieve the sensorless control for the OEW-PMSM system with the common dc bus, the zero-sequence model is adopted in [25] to extract motor angle and speed which is included in the zero-sequence voltage.

Two converters derived OEW-PMSM system can bring lots of benefits, but the problem with too many devices in topology structure still need to be faced [22]. Thus, the semi-controlled open-end winding PMSM control

system (SOEW-PMSM) fed by a uncontrolled converter and a controlled converter obtain a broader focus, due to the simpler topology structure, less power devices and easier control strategy. In order to increase the power output ability, literature [12] presents a series-compensation-based SOEW-PMSM generation system, which has good control performance. In the application of electrical vehicle, literature [13] developed an inverter-rectifier structure based on the SOEW-PMSM, which can be used in starter-generator system and extend the application scope of the OEW-PMSM. Under the condition of the SOEW-PMSM control system feeding by two isolated power sources, literature [14] analyzes the control effectiveness and the modulation ranges of different level of two power sources. In addition, the unity power factor control is implemented in this paper to gain optimal modulation index. On the other hand, under the condition of the SOEW-PMSM control system feeding by a common power source, zero-sequence circulation path is generated. Thus, in order to implement zero-sequence current (ZSC) suppression, literature [15], [16] added the ZSC control loop and designed zero-sequence modulation algorithm.

Above-mentioned control strategies are able to implement simultaneous control of the d-q axis current and the zero-sequence current, but the increase of the control complexity are inevitable due to extra ZCS control loop and modulation. In this paper, a simple prediction control strategy for SOEW-PMSM system based on the controllable side vector optimization is proposed, which can obtain satisfactory control performance. At first, the prediction model of this generation system is derived, and the current-voltage dual delay-compensation algorithm is presented to improve control performance of system. Then, the current error based cost function is designed. In addition, in order to further increase the steady-state control performance and reduce the computation burden, the improved current predictive control method based on the controllable side vector optimization is presented.
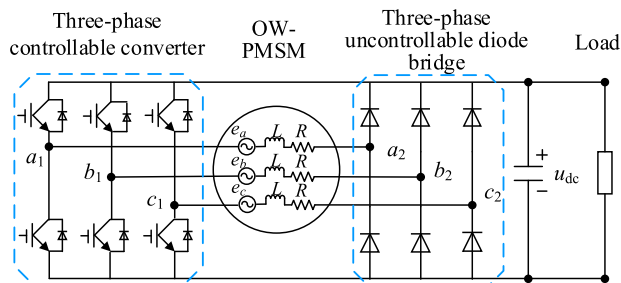

FIGURE 1. The control system structure.

II. SYSTEM MODEL

The Fig.1 shows the control construct of SOEW-PMSM system, which includes a controlled converter, an uncontrolled converter, an open-end winding motor and a load.

The model of SOEW-PMSM in *abc* frame is shown in (1) and (2); the model in *dq* frame and zero frame is

shown in (3) [16], [20], [27].

$$
\begin{cases}
u_a = u_{a1} - u_{a2} = e_a - L\dfrac{di_a}{dt} - i_a R \\[2mm]
u_b = u_{b1} - u_{b2} = e_b - L\dfrac{di_b}{dt} - i_b R \\[2mm]
u_c = u_{c1} - u_{c2} = e_c - L\dfrac{di_c}{dt} - i_c R
\end{cases} \tag{1}
$$

$$
\begin{cases}
e_a = -p\omega\psi_f \sin(\theta) \\
e_b = -p\omega\psi_f \sin(\theta - 2\pi/3) \\
e_c = -p\omega\psi_f \sin(\theta + 2\pi/3)
\end{cases} \tag{2}
$$

$$
\begin{cases}
u_d = u_{d1} - u_{d2} = -L_d\dfrac{di_d}{dt} - Ri_d - \omega L_q i_q \\[2mm]
u_q = u_{q1} - u_{q2} = -L_q\dfrac{di_q}{dt} - Ri_q - \omega L_d i_d + \omega\psi_f \\[2mm]
u_z = u_{z1} - u_{z2} = -L_z\dfrac{di_z}{dt} - Ri_z - 3\omega\psi_{f3}\sin(3\theta)
\end{cases} \tag{3}
$$

where, R represents stator resistance; u_{a1}, u_{b1} and u_{c1} represent controlled converter voltage; u_{a2}, u_{b2} and u_{c2} represent uncontrolled converter voltage. The *dq*-axis and the zero-axis inductance satisfies $L_d = L_q = L$ and $L_z = L - 2M$, in which M represents the mutual inductance.

Form the zero-sequence equation in (3), it can be obviously seen that the ZCS is mainly produced by two factors, i.e., the common model voltage generated by the controlled converter and the uncontrolled converter, and the third harmonic component in back EMF. Therefore, in order to reduce ZSC, the common model voltage u_z should be controlled to counteract the third harmonic component $3\omega\psi_{3f}\sin(3\theta)$.
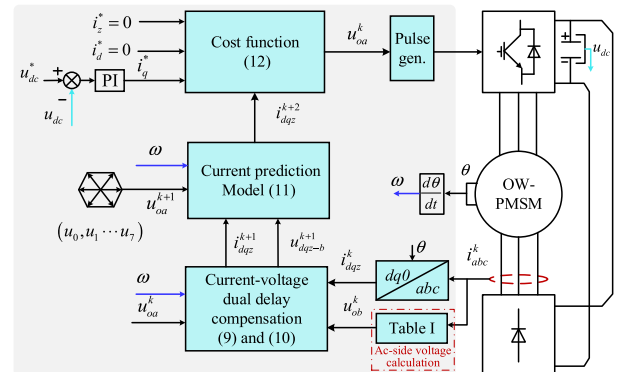

FIGURE 2. The control diagram of the proposed prediction method.

III. DUAL DELAY COMPENSATION BASED CURRENT PREDICTIVE CONTROL

A simple current prediction control method is presented in this paper, which avoid extra zero sequence current loop and complex modulation. The control diagram of this method is shown in Fig.2.

A. CURRENT PREDICTION

According to work principle of the uncontrolled converter, its output voltage depends on the phase current polarity.

Current direction			Vectors
i_a	i_b	i_c	
+	–	–	V_{uc4} (0 1 1)
+	+	–	V_{uc5} (0 0 1)
–	+	–	V_{uc6} (1 0 1)
–	+	+	V_{uc1} (1 0 0)
–	–	+	V_{uc2} (1 1 0)
+	–	+	V_{uc3} (0 1 0)

Therefore, the voltage of the uncontrolled converter in (1) is able to be expressed as [20], [26].

$$\begin{cases} u_{a2} = \dfrac{1 - \text{sgn}(i_a)}{2} u_{dc} = \begin{cases} u_{dc} & (i_a < 0) \\ 0 & (i_a > 0) \end{cases} \\[3mm] u_{b2} = \dfrac{1 - \text{sgn}(i_b)}{2} u_{dc} = \begin{cases} u_{dc} & (i_b < 0) \\ 0 & (i_b > 0) \end{cases} \\[3mm] u_{c2} = \dfrac{1 - \text{sgn}(i_c)}{2} u_{dc} = \begin{cases} u_{dc} & (i_c < 0) \\ 0 & (i_c > 0) \end{cases} \end{cases} \quad (4)$$

where u_{dc} represents the dc bus voltage, and sgn() represents sign function. From (4), it can be seen that eight different voltage vectors can be obtained theoretically in this uncontrolled converter due to eight different types of current direction. However, only six voltage vectors exist in the actual system, since three-phase current is not able to be in the same direction at one time. Table 1 list the vectors generated by the uncontrolled converter, in which "+" and "−" represent positive current and negative current, respectively [20], [26]. Thus, the voltage in synchronous rotating frame is able to be expressed by the Clark/Park transformation as

$$\begin{bmatrix} u_{d2} \\ u_{q2} \\ u_{z2} \end{bmatrix} = \frac{2}{3} \begin{bmatrix} 1 & -\dfrac{1}{2} & -\dfrac{1}{2} \\ 0 & \dfrac{\sqrt{3}}{2} & -\dfrac{\sqrt{3}}{2} \\ \dfrac{1}{2} & \dfrac{1}{2} & \dfrac{1}{2} \end{bmatrix}$$

$$\times \begin{bmatrix} \cos(\theta) & \sin(\theta) & 0 \\ -\sin(\theta) & \cos(\theta) & 0 \\ 0 & 0 & 1 \end{bmatrix} \begin{bmatrix} u_{a2} \\ u_{b2} \\ u_{c2} \end{bmatrix} \quad (5)$$

According to above models, a discrete-time prediction model of SOEW-PMSM can be obtained as

$$i_{dqz}^{k+1} = F(k) i_{dqz}^k + G[u_{oa}^k - u_{ob}^k] + H(k) \quad (6)$$

where $F(k) = \begin{bmatrix} 1 - \dfrac{T_s R}{L_d} & T_s \omega^k & 0 \\ -T_s \omega^k & 1 - \dfrac{T_s R}{L_q} & 0 \\ 0 & 0 & 1 - \dfrac{T_s R}{L_z} \end{bmatrix}$, $G = $

$\begin{bmatrix} \dfrac{T_s}{L_d} & 0 & 0 \\ 0 & \dfrac{T_s}{L_q} & 0 \\ 0 & 0 & \dfrac{T_s}{L_z} \end{bmatrix}$, $H(k) = \begin{bmatrix} 0 \\ \dfrac{\omega^k \psi_{1f} T_s}{L_q} \\ -\dfrac{3\omega_{3f} \sin(3\theta) T_s \omega^k}{L_z} \end{bmatrix}$ and u_{oa}^k and u_{ob}^k

are the voltage vectors of the controlled converter and the uncontrolled converter, respectively; T_s is the period.

B. CURRENT-VOLTAGE DUAL DELAY-COMPENSATION

In digital implementations, the existence of the one-step delay compensation is unavoidable, and it would impact the whole control performance. If this delay cannot be compensated correctly, the control performance of the whole system gets worse, especially under the condition of low sampling frequency [20]. Thus, correct one-step delay compensation of the SOEW-PMSM system is important for improving control performance. However, this control system is driven by dual converter, which causes the one-step delay compensation is different from the conventional compensation method. Therefore, according to the character of this SOEW-PMSM system, a current-voltage dual compensation strategy is proposed, which includes two parts, i.e., current one-step prediction of the whole control system and voltage one-step prediction of the uncontrollable converter.

1) CURRENT ONE-STEP PREDICTION

Similar to digital control implementation of the conventional PMSM system, this SOEW-PMSM system also needs to predict motor current of the next control period. Thus, prediction model (6) can be used to implement current prediction. However, in this system, it is worth highlighting that the prediction current not only is used to compensate current one-step delay, but also is adopted as condition to compensate voltage delay of the uncontrolled converter. Therefore, current prediction precision becomes a key factor to affect compensation effect of this SOEW-PMSM control system.

To improve the current prediction accuracy, second-order discrete model is used in this paper, which is shown as

$$\begin{cases} \hat{i}_{dqz}^{k+1} = F(k) i_{dqz}^k + G[u_{oa}^k - u_{ob}^k] + H(k) \\[2mm] i_{dqz}^{k+1} = \hat{i}_{dqz}^{k+1} + \dfrac{T_s R}{2 L_{dqz}} (\hat{i}_{dqz}^{k+1} - i_{dqz}^k) \end{cases} \quad (7)$$

The value of $\hat{i}_{dqz}^{k+1}$ is calculated by the first equation of (7) as a rough approximation of i_{dqz}^{k+1}, which is forward Euler integration part. In this part, the voltages generated by dual converter, i.e., u_{oa}^k and u_{ob}^k, need to be measured. And then, current $\hat{i}_{dqz}^{k+1}$ is used in the second equation of (7) to obtain more accurate prediction current i_{dqz}^{k+1}, this part is equivalent to trapezoidal integration method. Finally the prediction current i_{dqz}^{k+1} in compensation equation (7) is adopted to replace the sampled currents i_{dqz}^k in prediction model (6) and simultaneously is used as condition of voltage prediction for the uncontrollable diode bridge.

2) VOLTAGE ONE-STEP PREDICTION OF THE UNCONTROLLED CONVERTER

According to the compensation equation (7), the current of the next control period is able to be predicted, thus the phase current polarity can be adopted to predict the voltage of uncontrolled converter at $(k + 1)$th instant, which is

expressed as

$$
\begin{cases}
u_{a2}^{k+1} = \dfrac{1 - \mathrm{sgn}\left(i_a^{k+1}\right)}{2} u_{dc} = \begin{cases} u_{dc} & (i_a^{k+1} < 0) \\ 0 & (i_a^{k+1} > 0) \end{cases} \\[4mm]
u_{b2}^{k+1} = \dfrac{1 - \mathrm{sgn}\left(i_b^{k+1}\right)}{2} u_{dc} = \begin{cases} u_{dc} & (i_b^{k+1} < 0) \\ 0 & (i_b^{k+1} > 0) \end{cases} \\[4mm]
u_{c2}^{k+1} = \dfrac{1 - \mathrm{sgn}\left(i_c^{k+1}\right)}{2} u_{dc} = \begin{cases} u_{dc} & (i_c^{k+1} < 0) \\ 0 & (i_c^{k+1} > 0) \end{cases}
\end{cases} \tag{8}
$$

Then, the voltage u_{ob}^{k+1} of the uncontrolled converter in the synchronous rotating frame is able to be gained based on the Clark/Park transformation.

In order to compensate one-step delay, prediction model (6) needs to be updated by the voltage u_{ob}^{k+1} of the uncontrollable convertor and the current i_{dqz}^{k+1} according to (7) and (8), which is shown as

$$
i_{dqz}^{k+2} = F(k)i_{dqz}^{k+1} + G[u_{oa}^{k+1} - u_{ob}^{k+1}] + H(k) \tag{9}
$$

Therefore, the currents at $(k + 2)$th instant can be predicted with different voltage vector u_{oa}^{k+1} of the controlled converter. Fig.3 displays the structure diagram of the proposed compensation strategy.
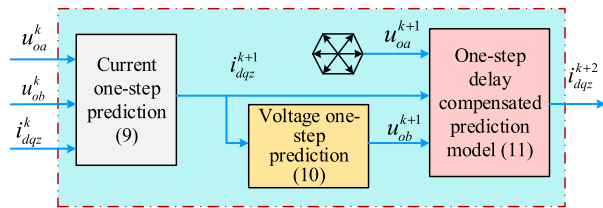
FIGURE 3. The structure diagram of the proposed compensation strategy.

C. VECTOR DISTRIBUTION AND SELECTION

Based on 6 basic voltage vectors of the uncontrolled converter and 8 basic voltage vectors provided by controlled converter, the vector distribution of this SOEW-PMSM system can be obtained. For example, if i_a is positive, while i_c and i_b are negative, vector V_{uc4} (011) can be generated by the uncontrolled convertor according to Table 1, which can be described by OD in the Fig. 4 (a). Similarly, vector $-V_{uc4}$ can be described by OA. Meanwhile, at point A, there are 8 voltage vectors can be generated by the controlled converter. It means that 8 basic voltage vectors ($V_0, V_1 \ldots V_7$) can be synthesized when three-phase current satisfies $i_a > 0$, $i_c < 0$ and $i_b < 0$, as shown as Fig. 4 (a). Similarly, if currents (i_a, i_b and i_c) satisfies different direction, different basic voltage vectors can be obtained. Then the whole vector distribution of this SOEW-PMSM system can be described as Fig.4 (b), which includes 24 nonzero vectors and 1 zero vector.

In this paper, in order to achieve simultaneous control of dq-axis current and the ZSC, the current errors based cost
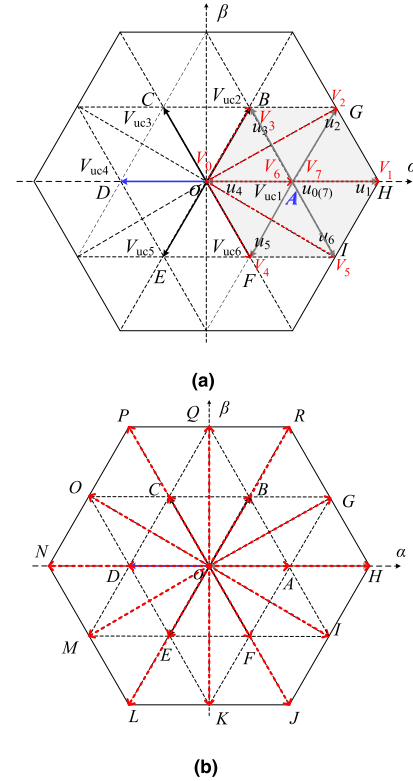
FIGURE 4. System vector distribution.

function is designed as follows

$$
J = \left| i_{dqz}^* - i_{dqz}(k + 2) \right| \tag{10}
$$

where i_{dqz}^* represents the current reference value. Then, the basic voltage vector that minimizes this cost function is selected as the best vector to apply for the motor.

According to the above analysis, it can be seen that it is very simple for this SOEW-PMSM system to implement simultaneous control of dq-axis current and ZSC by using this current prediction method, which avoids the use of three PI-based current loops and modulation strategy.

IV. IMPROVED PREDICTION CONTROL METHOD

Two voltage vectors used in one control period can improve the steady-state control performance of model predictive control system [18], [19]. Thus, this paper adopts the two vectors concept to improve the simultaneous control ability of dq-axis current and ZCS. It is worth noting that the control system in literature [18], [19] includes a 2-level converter, thus, 8 voltage vectors can be selected as candidate vector. However, for the SOEW-PMSM system, two converters generate high up to 25 basic voltage vectors. When two basic voltage vectors are used in every control period, the candidate vector combination will reach 625(25∗25). This means that it is very hard to achieve two vectors based prediction control in this SOEW-PMSM control system, since the vector selection is very complex and time consuming. Therefore, this paper presents a low computational complexity control strategy for

this SOEW-PMSM system based on the controllable side voltage vector optimization.

In this paper, the voltage vector selection of the SOEW-PMSM system is transferred to the voltage vector selection of the controlled converter by predicting expected voltage reference vector. Then, the candidate voltage vector combination is reduced from 625 to 42. Additionally, to aim at the controlled converter, to further optimize voltage vector and reduce computational complexity, $\alpha\beta$-plane-sector based vector selection strategy is presented in this session. Fig.5 displays the control block diagram of the proposed method.
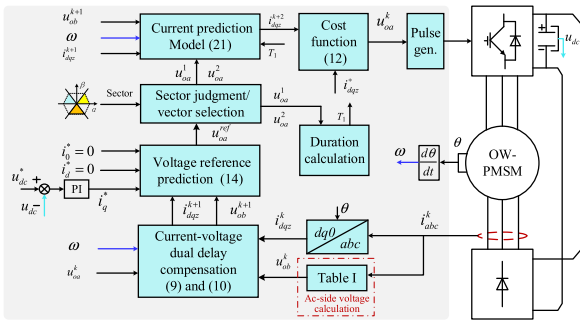

FIGURE 5. Control block diagram of this proposed prediction control strategy.

A. REFERENCE VOLTAGE PREDICTION OF CONTROLLED CONVERTER

To reduce system computation burden, the valid candidate range of voltage vector combination need to be decreased reasonably. Therefore, in this paper, the expected reference voltage of the controlled converter is predicted adopting the current deadbeat principle.

According to the basic deadbeat principle, when the predictive current i_{dqz}^{k+2} is equal to the current command i_{dqz}^*, which means that cost function (10) would reach zero at the end of the next control period, the expected voltage vector of the OW-PMSM system at the next control period can be predicted as [27]

$$u_{ref} = u_{oa}^{k+1} - u_{ob}^{k+1} = G^{-1} \cdot \left[i_{dqz}^* - F(k)i_{dqz}^{k+1} - H(k) \right] \quad (11)$$

where u_{ref} is the expected reference voltage of SOEW-PMSM system at the $(k+1)$th instant. This voltage vector can be used as the reference vector to select the candidate vector. But, the number of the candidate voltage vector combination under the control of dual vector prediction method would reach 625 (the first and second voltage vector both have 25 kinds of voltage selection, i.e.,$25 * 25 = 625$), when u_{ref} is used as reference vector. Therefore, in order to reduce the computational burden, the voltage selection target in this paper is changed from the whole SOEW-PMSM system to the controlled converter. Then, according to (11), the expected vector of the controlled converter at the next control period
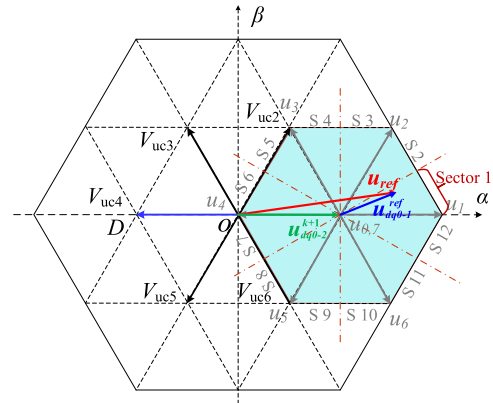

FIGURE 6. Sector distribution diagram.

can be predicted as

$$u_{oa}^{ref} = u_{ref} + u_{ob}^{k+1} = G^{-1} \cdot \left[i_{dqz}^* - F(k)i_{dqz}^{k+1} - H(k) \right] + u_{ob}^{k+1} \quad (12)$$

The relationship between u_{oa}^{ref} and the expected vector u_{ref} of the whole control system is shown in Fig.6. It can be seen that the controlled converter generates 8 basic voltage vectors (6 nonzero voltage vectors and 2 null voltage vectors), which means that the number of the candidate voltage vector combination under the control of dual vector prediction method would reach 42 (the first and second voltage vector have 6 and 7 kinds of voltage selection, respectively, i.e., $6 * 7 = 42$). Thus, the computational time of the voltage selection can be greatly reduced compared with 25 basic vectors provided by the whole OW-PMSM system.

B. VECTOR SELECTION

After obtaining the expected voltage vector of the controllable converter, its phase angle in $\alpha\beta$ frame is able to be easily calculated as

$$\theta = \arctan\left(u_\beta^{ref} \Big/ u_\alpha^{ref} \right) \quad (13)$$

where u_α^{ref} and u_β^{ref} represent α–axis and β–axis voltage of u_{oa}^{ref}. Based on this phase angle (13), the $\alpha\beta$ plane can be divided into twelve sectors, which are displayed in Fig.6. Three voltage vectors (2 zero voltage vectors and 1 nonzero vector) are contained in every sector. Then, the expected voltage vector can be used to determinate the candidate voltage vector combination according to the sector position of the phase angle. For example, if phase angle (13) satisfies $\theta \in (0°, 30°)$ at the current control period, it means that the expected voltage u_{oa}^{ref} is in the sector-1, while the first voltage vector of controlled converter should select nonzero vector u_1. In this case, it is obvious that the nonzero voltage vector u_2 is close to the expected vector u_{oa}^{ref}, thus, the second vector should be selected from nonzero vector u_2 and two null vectors u_0 and u_7. Similarly, voltage vectors should be determined based on this similar selection mode,

if the expected voltage u_{oa}^{ref} is in other sector. The relationship between the sector number and the candidate vector is given by Table 2.

TABLE 2. Sector distribution and selection relation of the first and the second voltage vector of controllable converter.

Sector	1	2	3	4	5	6	7	8	9	10	11	12
The first vector	u_1	u_2	u_2	u_3	u_3	u_4	u_4	u_5	u_5	u_6	u_6	u_1
The candidate second vector	u_0 u_2 u_7	u_0 u_1 u_7	u_0 u_3 u_7	u_0 u_2 u_7	u_0 u_4 u_7	u_0 u_3 u_7	u_0 u_5 u_7	u_0 u_4 u_7	u_0 u_6 u_7	u_0 u_5 u_7	u_0 u_1 u_7	u_0 u_6 u_7

According to aforementioned analysis, it can be seen that the proposed strategy for SOEW-PMSM system only need test 3 kinds of vector combination at every sector, which avoids evaluating all the vector combinations, and further reduces the system calculation load.

C. VECTOR APPLICATION TIME COMPUTATION

Since one system control period includes 2 vectors, application time of two vectors should be calculated. Therefore, the current slope needs to be obtained by the current differential equation (14) [27].

$$\frac{di_{dqz}}{dt} = -\frac{1}{L_{dqz}}\left(u_{oa} - u_{ob} + Ri_{dqz} + e_{dqz}\right) \quad (14)$$

Then, based on (14), the current slope s_1 of the SOEW-PMSM generated by selected first vector u_{oa}^1, and slope s_2 generated by second vector u_{oa}^2 can be calculated as [27]

$$s_1 = \frac{di_{dqz}}{dt} = -\frac{1}{L_{dqz}}\left(u_{oa}^1 - u_{ob} + Ri_{dqz} + e_{dqz}\right) \quad (15)$$

$$s_2 = \frac{di_{dqz}}{dt} = -\frac{1}{L_{dqz}}\left(u_{oa}^2 - u_{ob} + Ri_{dqz} + e_{dqz}\right) \quad (16)$$

Based on the slope s_1 and s_2, the current expression is able to be rewritten as

$$i_{dqz}^{k+2} = i_{dqz}^{k+1} + s_1 T_1 + s_2(T_s - T_1) \quad (17)$$

where T_1 and T_s-T_1 are the application time of the first and second vector, respectively. And then according to current deadbeat principle, i.e., $i_{dqz}^{k+2} = i_{dqz}^*$, the application time T_1 is able to be calculated as below [27]

$$T_1 = \frac{\left[i_{dqz}^* - i_{dqz}^{k+1} - s_1 T_s\right] \cdot (s_1 - s_2)}{(s_1 - s_2)^2} \quad (18)$$

Next, substituting the first voltage vector and its application time T_1 into prediction model (19) is able to predict the $dq0$-axis current of the three candidate second vectors [27].

$$i_{dqz}^{k+2} = F(k)i_{dqz}^{k+1} + \frac{T_1}{T_s}Gu_{oa}^1 + (1 - \frac{T_1}{T_s})Gu_{oa}^2 - Gu_{ob} + H(k) \quad (19)$$

Finally, the cost function (10) is used to test every candidate second vector and the vector that has minimum cost function value is considered as the best second vector.
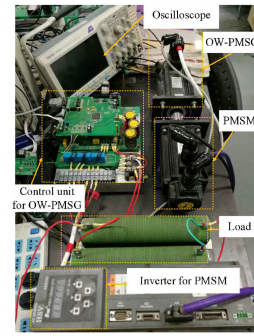

FIGURE 7. Experimental platform of OW-PMSM generation system.

TABLE 3. Parameters of system.

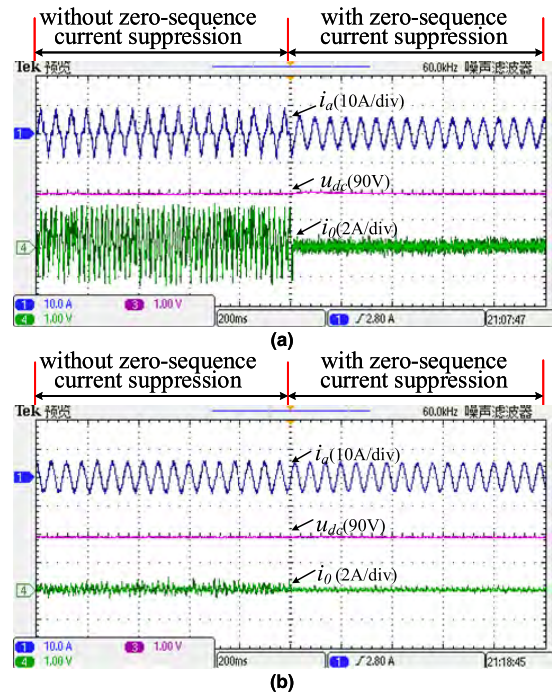|	
d- and q-axes inductances	$L_d = L_q = 5.292$mH
Zero sequence inductance	$L_0 = 4.3$mH
Stator phase resistance	$R = 1.5\Omega$
Number of pole pairs	$P = 2$
Load resistance	$R_L = 50\Omega$
Flux linkage of permanent magnets	$\psi_{f0} = 0.2404$Wb

FIGURE 8. Comparison results of the ZSC, (a) Method-I, (b) Method-II.

V. EXPERIMENTAL VERIFICATION

In order to test the validity of the proposed methods, experimental platform was built, as shown as Fig.7. The SOEW-PMSM parameters are given in the TABLE-3. In this paper, for simplicity, the proposed control strategy with dual delay compensation is named as Method-I, the proposed control strategy with controllable side vector optimization is named as Method-II, and the control method proposed by paper [20] is named Method-III.

The experimental results of the Method-I and Method-II are shown in Fig.8 and 9, which prove that the existence of the ZSC can lead to large current ripple. In addition, from the
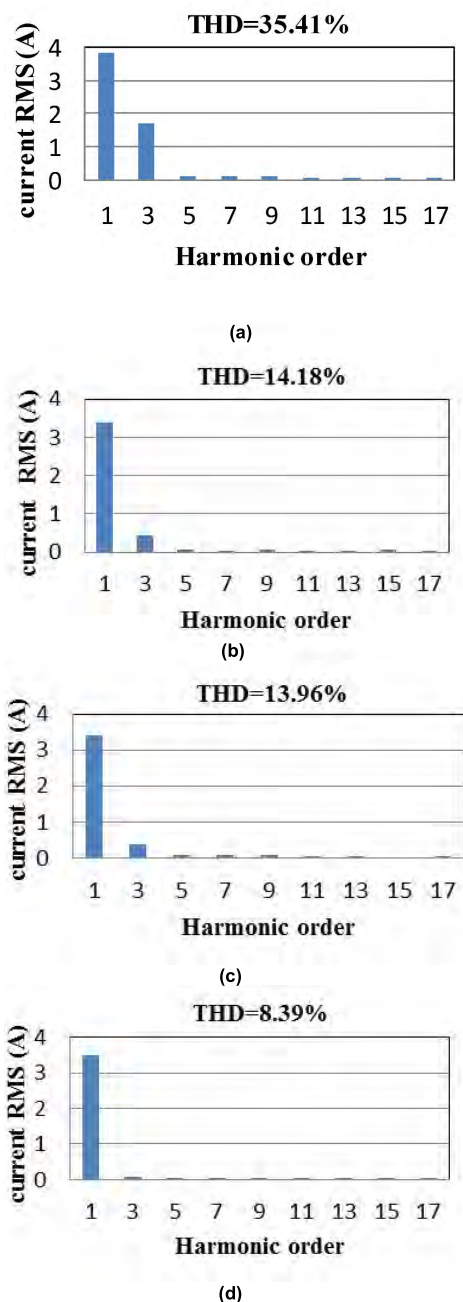
FIGURE 9. THD comparisons of phase current, (a) Method-I without ZSC suppression, (b) Method-II without ZSC suppression, (c) Method-I with ZSC suppression, (d) Method-II with ZSC suppression.

comparison test of Fig.9 (a) and (b), it is seen that the ZCS has less influence under the control of the Method-II, compared with the Method-I.

On the other hand, the current waveform can be significantly improved when the ZSC is suppressed. Under the control of the Method-I method, current harmonic is reduced to 13.96%; and under the control of the Method-II method, current harmonic is reduced to 8.39%. From above analyses, it is proved that Method-II has better ZSC control ability than the Method-I.

The steady-state performance comparison of three methods is given by Fig.10, in which the SOEW-PMSM speed and DC voltage command are set as 500r/min and 90V, respectively. From Fig.10 (a) and (d), it is shown that high ripple exists in the current waveform and the fluctuation of ZSC is about ± 1.2A, when the Method-I is used in this system. From Fig.10 (c) and (f), it is shown that when Method-III (paper [20]) is used, the ZSC fluctuates at ± 0.6A. However, On the other hand, according to Fig.10 (b) and (e), it is obvious that when the generation system is controlled by the Method-II, the whole control performances are improved significantly. Especially, the ZSC drops by 61.6% from 1.2 A to 0.46 A. Thus, the above-mentioned experimental results prove that excellent current control ability can be obtained under the control of three methods. However, by comparison, Method-II can gain better steady state control performance.

In order to compare the dynamic control performance, the control response results of three different methods are displayed in Fig.11 under the condition of dc voltage mutation. The experimental results show that three methods have excellent tracking control ability and good dynamic performance.

Additionally, experimental results when resistance and inductance parameter mismatches exist in the control system are given in Figs.12 and 13 with the sudden change of the dc-voltage command. Fig.12 shows the dq-axis current and their responses when resistance exists mismatch. From experimental results, it is seen that resistance mismatches have no obvious influence on control performance, when Method-I, Method-II and Method-III are applied for this generation system, respectively. Fig.13 shows the dq-axis current and their responses when inductance exists mismatch. From this waveform, it is obvious that when inductance used in the model is larger than the actual value of the motor, three methods would cause the increase of the current ripple. On the other hand, when inductance parameter used in the model is smaller than the actual value, the Method-I and Method-III both causes a little current static error; however, this current tracking error caused by inductance mismatch is not obvious by the control of the Method-II. Therefore, from experimental results of the Figs.12 and 13, it is obvious that three methods have suppression ability when parameter mismatches occur, however, Method-II has better suppression effect compared with Method-I and Method-III.

In order to further validate the proposed method (Method-II), the three-phase current and ZSC waveforms of three different methods are shown in Fig.14 when dc voltage reference is suddenly changed from 90V to 50V. It is obvious that the current control performances of the proposed Method-II better than that of other methods.

Fig.15 shows that dynamic responses of dc bus voltage and motor currents under the condition of prime mover speed variation. It is obvious that three methods have good dc voltage tracking characteristic. Additionally, the torque responses are tested in this paper, when three different methods are used with dc voltage command sudden change (According to power balance principle between AC side and DC side in
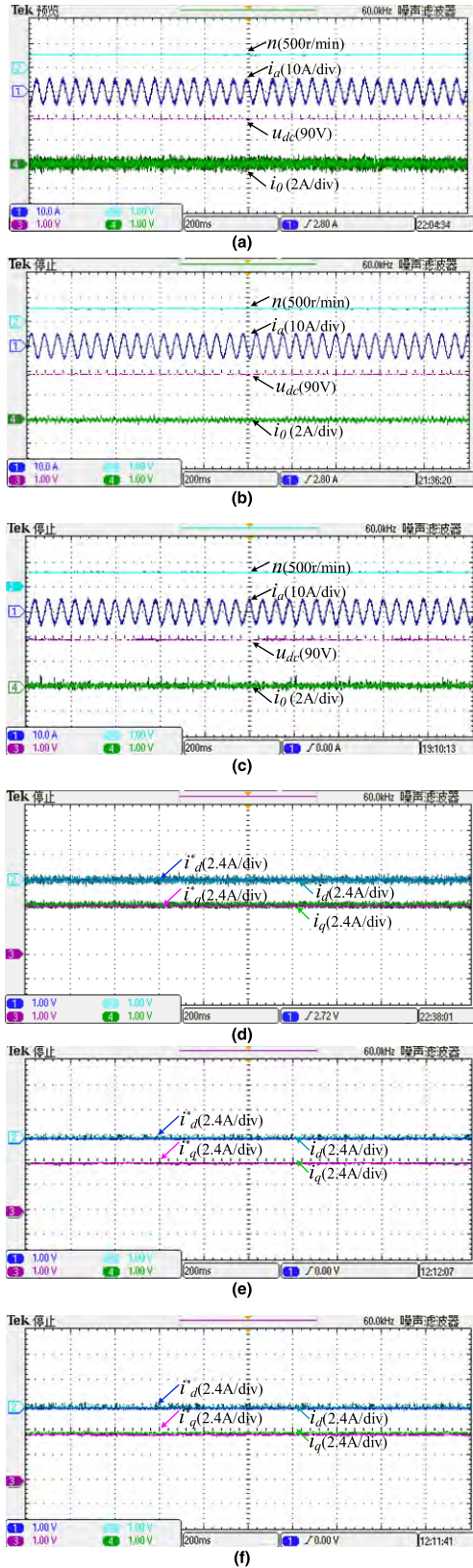
FIGURE 10. Steady-state experimental results at speed of 500r/min. (a) Method-I. (b) Method-II. (c) Method-III. (d) Method-I. (e) Method-II. (f) Method-III.
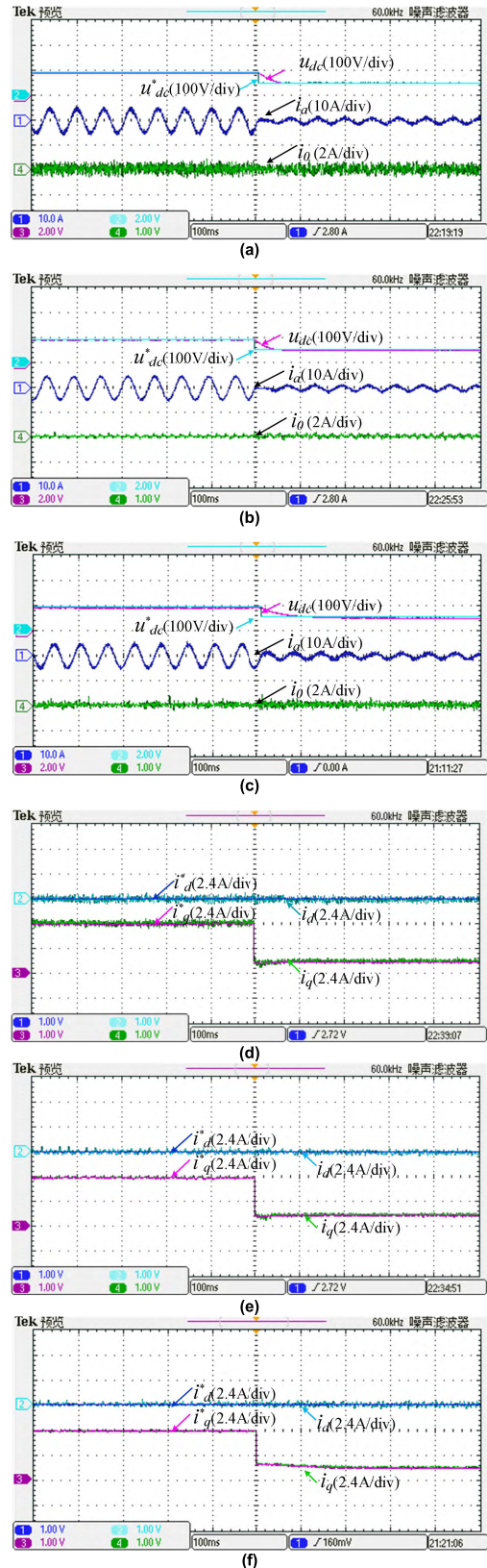

FIGURE 11. Dynamic performance comparison, (a) Method-I, (b) Method-II, (c) Method-III, (d) Method-I, (e) Method-II, (f) Method-III.
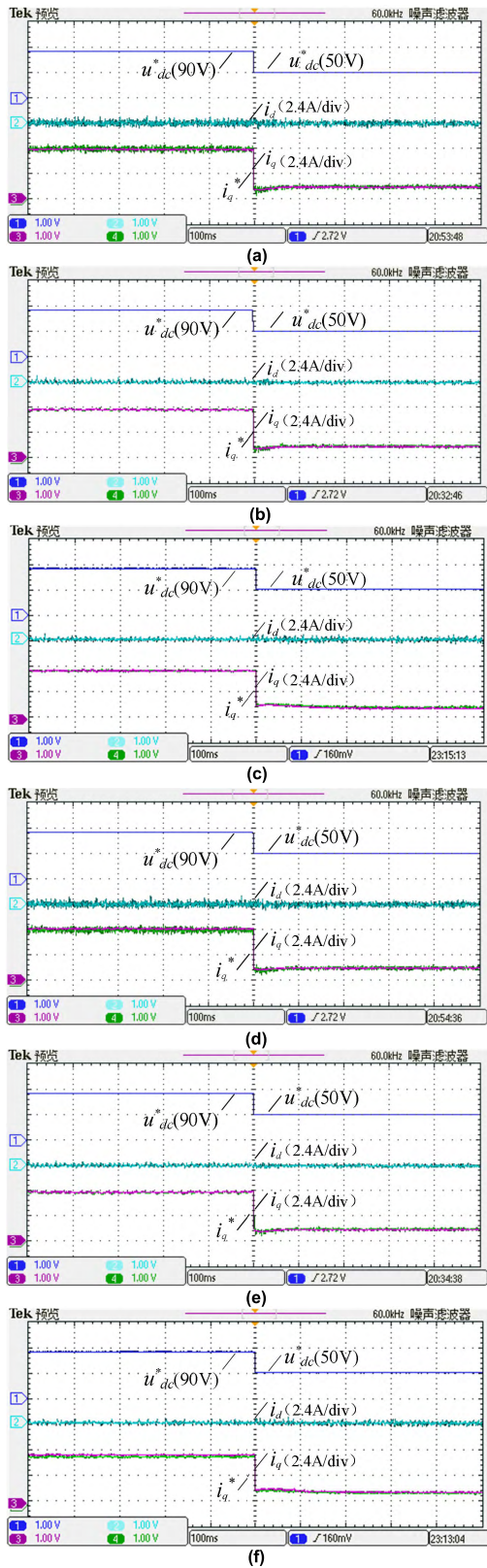
FIGURE 12. Experimental results of resistance parameter mismatch (a) R = 1.5RM in Method-I (b) R = 1.5RM in Method-II (c) R = 1.5RM in Method-III (d) R = 0.5RM in Method-I (e) R = 0.5RM in Method-II (f) R = 0.5RM in Method-III (RM is the actual resistance of the motor).
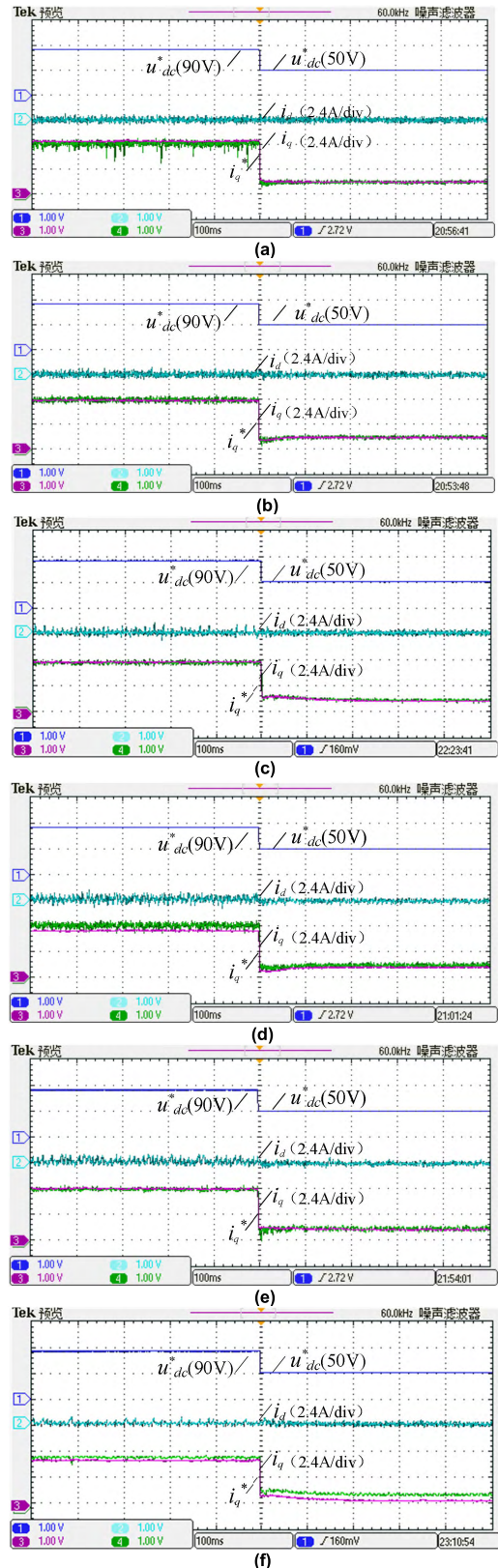

FIGURE 13. Experimental results of inductance parameter mismatch (a) L = 1.5LM in Method-I (b) LM = 1.5LM in Method-II (c) LM = 1.5LM in Method-III (d) L = 0.5LM in Method-I (e) L = 0.5LM in Method-II (f) L = 0.5LM in Method-III (LM is the actual inductance of the motor).
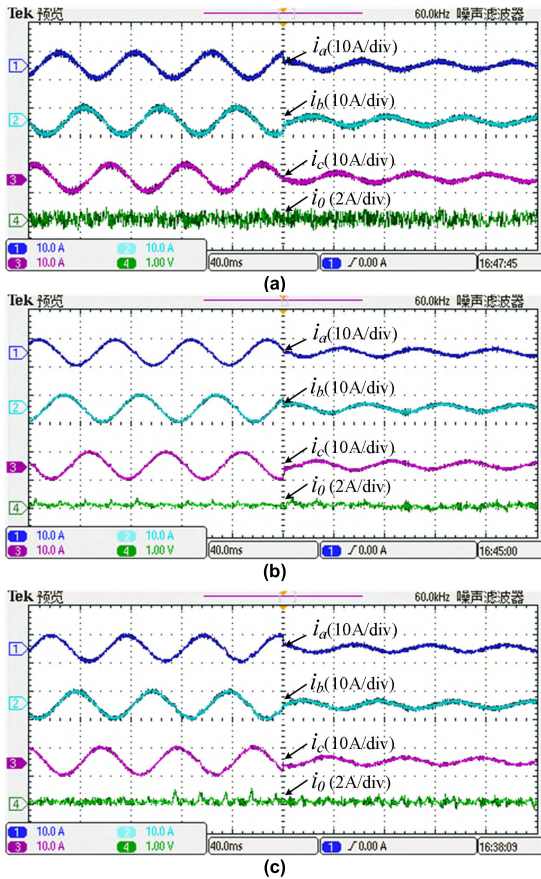
FIGURE 14. Current waveform when dc bus voltage reference changes, (a) Method-I, (b) Method-II, (c) Method-III.

generation system, i.e., $T_e*n/9550 = P = u_{dc}*u_{dc}/R$, dc voltage u_{dc} variation is equivalent to the torque T_e variation under condition of the same speed and load.). The test results are shown in the Fig.16, which indicates that three different methods have quick dynamic response and good disturbance rejection performance.

Additionally, the calculation time comparison is given, when Method-I and Method-II are adopted, respectively. The Method-I requires 45.02*u* s to complete code operation, and the calculation time of proposed Method-II in this paper is reduced to 41.59*u* s. It indicates that the algorithm calculation time can be effectively reduced by the proposed Method-II. On the other hand, the method proposed in paper [20] (named Method-III) also is carried out to compare with the proposed method. The average calculation time of the Method-III is 40.76*u* s. The comparison results reveal that the Method-II needs a bit more calculation time compared with Method-III. The reason is that candidate voltage vectors of the Method-II is 3, however, Method-III needs select optimal vector from 1 candidate voltage vector, 2 candidate vectors or 4 candidate vectors in a control period according to different voltage sector. Although the proposed method needs more calculation load compared with literature [20], the better control performance can be obtained.
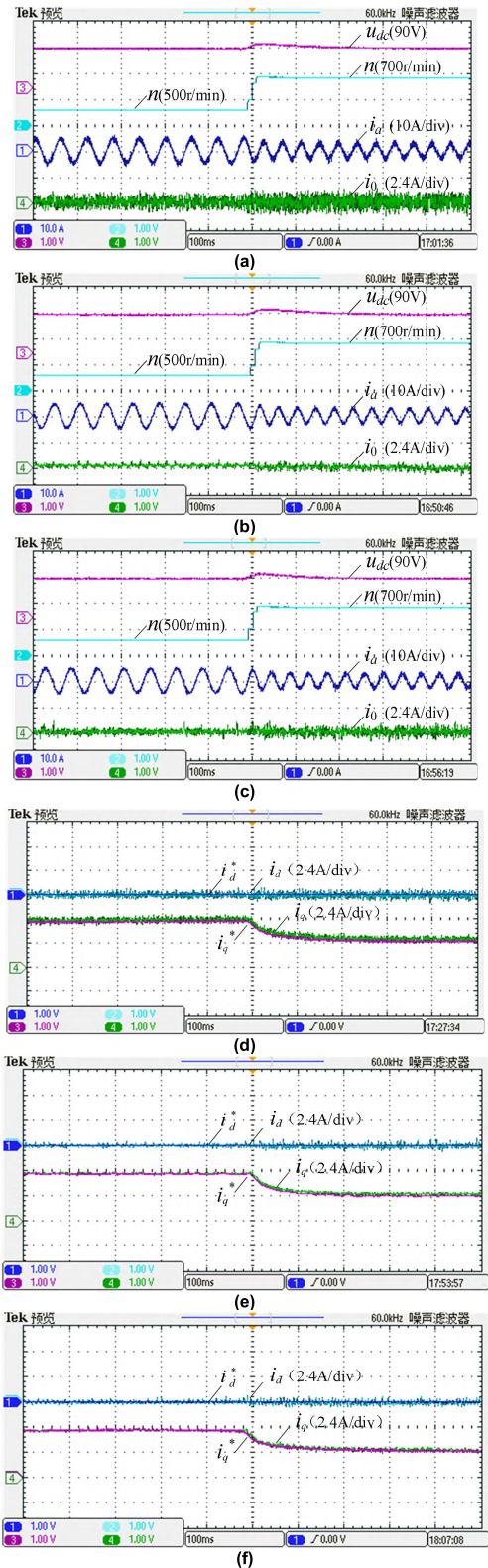

FIGURE 15. Dynamic responses of dc bus voltage and motor currents with speed variation, (a) Method-I, (b) Method-II, (c) Method-III, (d) Method-I, (e) Method-II, (f) Method-III.

In order to compare different methods more intuitively, the experimental results shown in this paper are quantitatively provided in the TABLE 4.
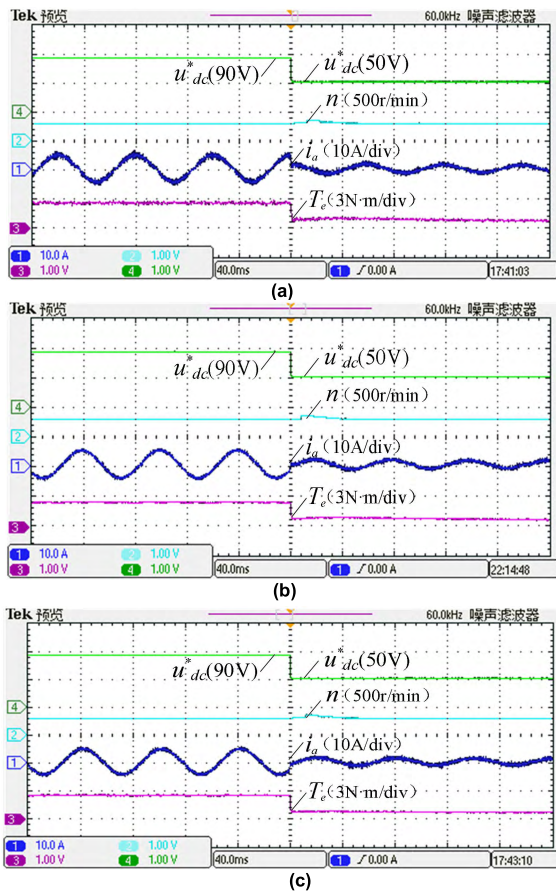
FIGURE 16. The torque variation test at the speed of 500r/min, (a) Method-I, (b) Method-II, (c) Method-III.

TABLE 4. Control performance comparison of the different methods.

Performances \ Method	Method-I	Method-II	Method-III
Steady-state performance (Zero-sequence current fluctuation)	Large (1.2A)	Small (0.46A)	Medium (0.6A)
Dynamic performance (voltage tracking time)	Good (55ms)	Good (50ms)	Good (55ms)
Control performance with parameter mismatches (maximum static error)	Bad (0.48A)	Good (0)	Medium (0.38A)
Computation burden	High (45.02us)	Medium (41.59us)	Low (40.76us)

In order to test the effectiveness of the proposed control method at high speed and high current conditions, the experimental results at the condition of rated speed and rated torque are given by Fig.17. The experimental results further verify the effectiveness of the proposed methods under the condition of rated speed and rated torque.

In summary, all above results indicate that under the control of the three methods, the zero-sequence current existed in the SOEW-PMSM system can be suppressed effectively. Compared with Method-I, the proposed Method-II has better
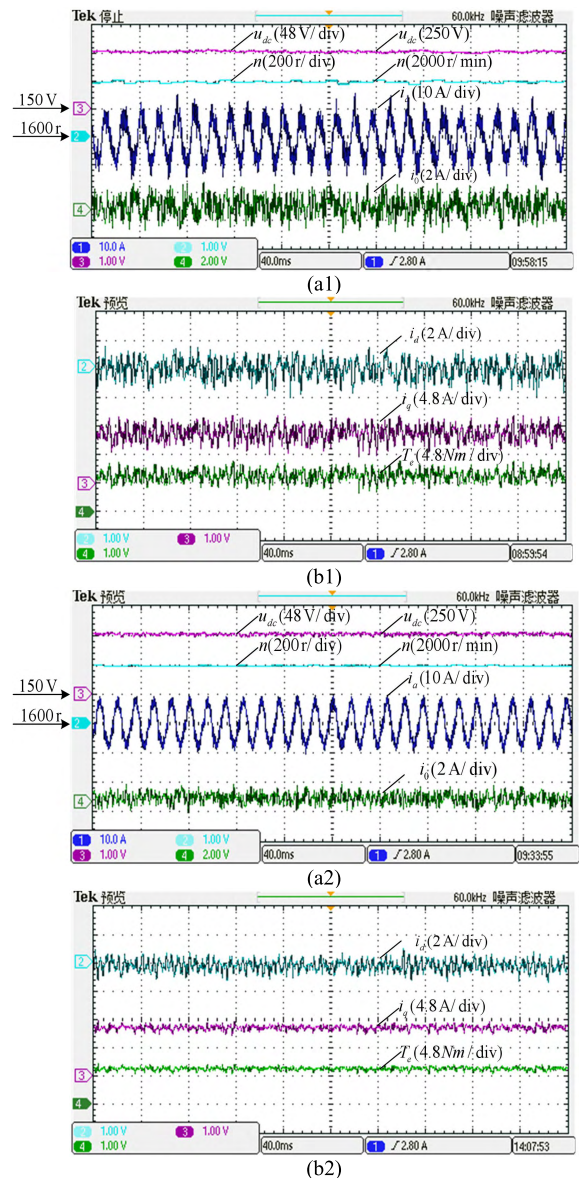

FIGURE 17. Steady-state experiment results at the rated speed and rated torque, (a1) (b1) MPCC-I method, (a2) (b2) MPCC-II method.

steady-state control performance, better parameter robustness and lower computation burden. Compared with Method-III, although the proposed Method-II needs more computation time, the better control performance and the better parameter robustness can be obtained.

VI. CONCLUSION
In this paper, a simple prediction control for SOEW-PMSM system is presented, which avoid the use of three current controllers and extra modulation design for the zero-sequence suppression; moreover, the dual delay compensation strategy is proposed in this paper to improve the control performance; furthermore, the control method based on the controllable side vector optimization is presented to reduce the computation burden and further improve the steady-state control performance.

REFERENCES

[1] A. P. Sandulescu, F. Meinguet, X. Kestelyn, E. Semail, and A. Bruyere, "Flux-weakening operation of open-end winding drive integrating a cost-effective high-power charger," *IET Electr. Syst. Transp.*, vol. 3, no. 1, pp. 10–21, Mar. 2013.

[2] G. Wang, R. Yang, and D. Xu, "DSP-based control of sensorless IPMSM drives for wide-speed-range operation," *IEEE Trans. Ind. Electron.*, vol. 60, no. 2, pp. 720–727, Feb. 2013.

[3] V. T. Somasekhar, K. Gopakumar, M. R. Baiju, K. K. Mohapatra, and L. Umanand, "A multilevel inverter system for an induction motor with open-end windings," *IEEE Trans. Ind. Electron.*, vol. 52, no. 3, pp. 824–836, Jun. 2005.

[4] V. T. Somasekhar, S. Srinivas, and K. K. Kumar, "Effect of zero-vector placement in a dual-inverter fed open-end winding induction-motor drive with a decoupled space-vector PWM strategy," *IEEE Trans. Ind. Electron.*, vol. 55, no. 6, pp. 2497–2505, Jun. 2008.

[5] G. Mondal, K. Sivakumar, R. Ramchand, K. Gopakumar, and E. Levi, "A dual seven-level inverter supply for an open-end winding induction motor drive," *IEEE Trans. Ind. Electron.*, vol. 56, no. 5, pp. 1665–1673, May 2009.

[6] B. V. Reddy, V. T. Somasekhar, and Y. Kalyan, "Decoupled space-vector PWM strategies for a four-level asymmetrical open-end winding induction motor drive with waveform symmetries," *IEEE Trans. Ind. Electron.*, vol. 58, no. 11, pp. 5130–5141, Nov. 2011.

[7] G. Mondal, K. Gopakumar, P. N. Tekwani, and E. Levi, "A reduced-switch-count five-level inverter with common-mode voltage elimination for an open-end winding induction motor drive," *IEEE Trans. Ind. Electron.*, vol. 54, no. 4, pp. 2344–2351, Aug. 2007.

[8] Q. An, J. Liu, Z. Peng, L. Sun, and L. Sun, "Dual-space vector control of open-end winding permanent magnet synchronous motor drive fed by dual inverter," *IEEE Trans. Power Electron.*, vol. 31, no. 12, pp. 8329–8342, Dec. 2016.

[9] A. Edpuganti and A. K. Rathore, "New optimal pulsewidth modulation for single DC-link dual-inverter fed open-end stator winding induction motor drive," *IEEE Trans. Power Electron.*, vol. 30, no. 8, pp. 4386–4393, Aug. 2015.

[10] C. Patel, R. P. P, A. Dey, R. Ramchand, K. Gopakumar, and M. P. Kazmierkowski, "Fast direct torque control of an open-end induction motor drive using 12-sided polygonal voltage space vectors," *IEEE Trans. Power Electron.*, vol. 27, no. 1, pp. 400–410, Jan. 2012.

[11] S. Chowdhury, P. W. Wheeler, C. Gerada, and C. Patel, "Model predictive control for a dual-active bridge inverter with a floating bridge," *IEEE Trans. Ind. Electron.*, vol. 63, no. 9, pp. 5558–5568, Sep. 2016.

[12] D. Pan and T. A. Lipo, "Series compensated open-winding PM generator wind generation system," in *Proc. 15th Int. Conf. EPE/EPMC*, Sep. 2012, pp. LS7c.1-1–LS7c.1-8.

[13] J. Wei, Q. Deng, B. Zhou, M. Shi, and Y. Liu, "The control strategy of open-winding permanent magnet starter-generator with inverter-rectifier topology," *IEEE Trans. Ind. Informat.*, vol. 9, no. 2, pp. 983–991, May 2013.

[14] H. Nian and Y. Zhou, "Investigation of open-winding PMSG system with the integration of fully controlled and uncontrolled converter," *IEEE Trans. Ind. Appl.*, vol. 51, no. 1, pp. 429–439, Jan./Feb. 2015.

[15] H. Nian and Y. Zhou, "Investigation and suppression of current zero crossing phenomenon for a semicontrolled open-winding PMSG system," *IEEE Trans. Power Electron.*, vol. 32, no. 1, pp. 602–612, Jan. 2017.

[16] H. Nian, Y. Zhou, and H. Zeng, "Zero-sequence current suppression strategy for open winding PMSG fed by semicontrolled converter," *IEEE Trans. Power Electron.*, vol. 31, no. 1, pp. 711–720, Jan. 2016.

[17] Y. Zhang and H. Yang, "Model predictive torque control of induction motor drives with optimal duty cycle control," *IEEE Trans. Power Electron.*, vol. 29, no. 12, pp. 6593–6603, Dec. 2014.

[18] X. Zhang and B. Hou, "Double vectors model predictive torque control without weighting factor based on voltage tracking error," *IEEE Trans. Power Electron.*, vol. 33, no. 3, pp. 2368–2380, Mar. 2018.

[19] S. A. Davari, D. A. Khaburi, and R. Kennel, "An improved FCS–MPC algorithm for an induction motor with an imposed optimized weighting factor," *IEEE Trans. Power Electron.*, vol. 27, no. 3, pp. 1540–1551, Mar. 2012.

[20] X. Zhang and K. Wang, "Current prediction based zero sequence current suppression strategy for the semicontrolled open-winding PMSM generation system with a common DC bus," *IEEE Trans. Ind. Electron.*, vol. 65, no. 8, pp. 6066–6076, Aug. 2018.

[21] W. Hu, H. Nian, and T. Zheng, "Torque ripple suppression method with reduced switching frequency for open-winding PMSM drives with common DC bus," *IEEE Trans. Ind. Electron.*, vol. 66, no. 1, pp. 674–684, Jan. 2019.

[22] S. Lakhimsetty, N. Surulivel, and V. T. Somasekhar, "Improvised SVPWM strategies for an enhanced performance for a four-level open-end winding induction motor drive," *IEEE Trans. Ind. Electron.*, vol. 64, no. 4, pp. 2750–2759, Apr. 2017.

[23] M. Chen and D. Sun, "A unified space vector pulse width modulation for dual two-level inverter system," *IEEE Trans. Power Electron.*, vol. 32, no. 2, pp. 889–893, Feb. 2017.

[24] S. Srinivas and J. Kalaiselvi, "Pulse width modulation schemes enabling single DC power source driven dual two-level voltage source inverter with single voltage source inverter switching," *IET Power Electron.*, vol. 7, no. 5, pp. 1181–1191, May 2014.

[25] H. Zhan, Z. Q. Zhu, M. Odavic, and Y. Li, "A novel zero-sequence model-based sensorless method for open-winding PMSM with common DC bus," *IEEE Trans. Ind. Electron.*, vol. 63, no. 11, pp. 6777–6789, Nov. 2016.

[26] X. Zhang and K. Wang, "Model predictive current control for the semi-controlled open winding PMSG," in *Proc. 20th Int. Conf. Electr. Mach. Syst. (ICEMS)*, Sydney, NSW, Australia, Aug. 2017, pp. 1–5.

[27] X. Zhang, W. Zhang, and K. Wang, "Double vector model predictive current control for the semi-controlled open-winding PMSG generation system," in *Proc. IEEE Int. Power Electron. Appl. Conf. Expo. (PEAC)*, Nov. 2018, pp. 1–5.

XIAOGUANG ZHANG was born in 1985. He received the B.S. degree in electrical engineering from the Heilongjiang Institute of Technology, Harbin, China, in 2007, and the M.S. and Ph.D. degrees in electrical engineering from the Harbin Institute of Technology, in 2009 and 2014, respectively.

He is currently a Distinguished Professor with the North China University of Technology. From 2012 to 2013, he was a Research Associate with Wisconsin Electric Machines and Power Electronics Consortium (WEMPEC), University of Wisconsin–Madison, Madison. He has published more than 40 technical papers in the area of motor drives. His current research interests include power electronics and electric machines drives.

KEQIN WANG was born in Henan, China, in 1991. He received the B.S. degree in electrical engineering from the Henan Institute of Science and Technology, Henan, in 2015, and the M.S. degree in electrical engineering from the North China University of Technology, in 2018. He is currently with Jing-Jin Electric, Beijing, China. His current research interest includes permanent magnet synchronous motor drives.

WENHAN ZHANG was born in 1996. He received the B.S. degree in electrical engineering from the North China University of Technology, Beijing, China, in 2017, where he is currently pursuing the M.S. degree. His current research interest includes permanent magnet synchronous motor drives.

YAOQIANG WANG was born in 1982. He received the B.Sc. degree in measurement and control technology and instruments from Hangzhou Dianzi University, Hangzhou, China, in 2006, and the M.Sc. and Ph.D. degrees in electrical engineering from the Harbin Institute of Technology, Harbin, China, in 2008 and 2013, respectively.

He is currently an Associate Professor with the School of Electrical Engineering, Zhengzhou University, Zhengzhou, China. His research interests include power conversion technique and its applications in distributed generation, motor drive and flexible power transmission and distribution, and so on.

PENG WANG was born in 1982. He received the B.S. degree in electrical engineering from the Taiyuan University of Technology, Taiyuan, China, in 2008, and the M.S. degree in electrical engineering from the North China University of Technology, Beijing, China, in 2011.

Since 2011, he has been a Lecturer with the Inverter Technologies Engineering Research Center of Beijing, North China University of Technology. His current research interests include power electronics and electric machines drives.

DAWEI GAO received the B.S. degree in electrical engineering from Southwest Jiao Tong University, Chengdu, China, in 1992, and the Ph.D. degree in electrical engineering from North China Electric Power University, in 2001. He is currently an Associate Research Fellow with Tsinghua University. His current research interests include power electronic technology and electric drive control of automobile.

● ● ●